IOP Publishing | Vietnam Academy of Science and Technology Advances in Natural Sciences: Nanoscience and Nanotechnology

Adv. Nat. Sci.: Nanosci. Nanotechnol. **14** (2023) 025010 (8pp) https://doi.org/10.1088/2043-6262/acd684

Effect of Ar-plasma treatment and annealing on thermally evaporated β-In_2S_3 thin films

S Rasool[1,*], K Saritha[2], K T Ramakrishna Reddy[3], M S Tivanov[4], O V Korolik[4], V F Gremenok[5], S P Zimin[6,7] and I I Amirov[7]

[1] Faculty of Physics, Department of Basic Sciences & Humanities, Siddartha Institute of Science and Technology, Puttur—517 583, India
[2] Faculty of Physics, Department of Humanities & Basic Sciences, Chadalawada Ramanamma Engineering College, Tirupati—517 506, India
[3] Solar Photovoltaic laboratory, Department of Physics, Sri Venkateswara University, Tirupati—517 502, India
[4] Faculty of Physics, Belarusian State University, Nezavisimosti 4 av., 220030 Minsk, Belarus
[5] Scientific and Practical Materials Research Centre, National Academy of Sciences,220072 Minsk, Belarus
[6] Microelectronics and General Physics Department, P.G. Demidov Yaroslavl State University, 150003 Yaroslavl, Russia
[7] Yaroslavl Branch of the Valiev Institute of Physics and Technology, Russian Academy of Sciences, 150007 Yaroslavl, Russia

E-mail: rasool265@gmail.com and ktrkreddy@gmail.com

Received 17 August 2022
Accepted for publication 8 February 2023
Published 25 May 2023

Abstract

In the present study, the effect of annealing and Ar-plasma treatment on structural, morphological and optical properties of thermally evaporated β-In_2S_3 thin films has been investigated. During Ar-plasma treatment, some interesting results were observed that an array of metallic indium nanostructures was formed over In_2S_3 film surface with quasi-spherical or spread droplet shapes of an average size of 20–100 nm in the lateral direction and a height of less than 70 nm. Here, the Ar-plasma treatment serves as a new strategy for the self-formation of metallic indium nanostructures over the film surface. Further, the optical absorption of In_2S_3 films has been enhanced from 10^4 to 10^7 cm^{-1} while the optical band gap energy decreased from 2.71 eV to 2.50 eV after Ar-plasma treatment. The metallic nanostructures loaded on semiconductor surface can act as an electron trap that can effectively prevent the recombination of photo-generated electron-hole pairs.

Keywords: In_2S_3 thin films, annealing, argon plasma, indium nanostructures, physical properties
Classification numbers: 2.09, 4.00, 4.10, 5.00

1. Introduction

Indium sulphide (In_2S_3) is one of the potential materials used for photovoltaic and photocatalytic applications due to its optimal direct band gap energy (2.1 eV–2.7 eV), high optical absorption coefficient, n-type conductivity, high photo-conducting and eco-friendly nature [1–3]. β-In_2S_3 has defect spinel structure (cubic or tetragonal), in which cubic β-In_2S_3 has disordered indium vacancies, whereas tetragonal β-In_2S_3 has ordered vacancies. The disordered vacancies of cubic β-In_2S_3 can act as electron traps and hence drive the photo-catalysis process [4, 5].

Metallic nanostructures have ability to produce surface plasmon resonance (SPR) which is an effective way to improve the light trapping mechanism in optoelectronic devices. Plasmonic nanostructures composed of noble metal nanoparticles (e.g., Ag, Au and Pt) have been widely employed in a large range of applications, such as solar cells [6–8], photocatalysts [9, 10], light emitting diodes (LEDs) [11, 12], photoelectrochemical (PEC) cells [13] and photo-detectors [14] due to the high density of electrons. However, due to the scarcity and high cost of noble metals, researchers

* Author to whom any correspondence should be addressed.

showed much interest in plasmonic materials composed of non-noble metal nanoparticles (e.g., Cu, In, Sn and Al) [15]. In the present work, we observed the formation of metallic indium nanostructures on the β-In_2S_3 film surface during Ar-plasma treatment. The semiconductor photoelectrodes decorated with certain metal nanoparticles is an effective route for enhancing the photo-generated charge carrier separation. Usually, the metal nanoparticles have lower Fermi energy than the semiconductors, so that it can boost the electron transfer mechanism through Schottky contact. Consequently, the lifetime of photogenerated charge carriers can be extended. Wang *et al* [16] prepared Cd/CdS photocatalyst by chemical methods and observed that metal Cd can act as co-catalyst loaded on the CdS. In their study, Cd/CdS photocatalyst effectively reduced the recombination of photo-generated charge carriers.

Plasma treatment is an effective way to modify the physical and chemical properties of the material surface. Since the penetration depth of the ions of plasma into the sample is only a few nanometers, hence the surface properties of the materials can be immensely enhanced. Particularly, radio frequency (RF) plasma systems have ability to treat the surfaces more homogenously than other systems. During plasma treatment, high energetic Ar ions bombard the sample surface and break the existing chemical bonds between the surface atoms and induce the sputtering of lighter atoms from the material surface, leading to a change in its characteristic behaviour compared to untreated material.

The aim of the present work is to make a comparative study on the physical properties of In_2S_3 thin films between Ar-plasma treated and untreated films. Initially, β-In_2S_3 thin films were deposited using thermal evaporation technique and the as-deposited films were annealed in sulphur ambient. Later, the sulphur annealed films were treated with argon (Ar) plasma using RF inductively coupled plasma (ICP). Further, the structural, morphological and optical properties of these plasma treated films were studied and compared with untreated films. Through our studies, it is observed that the Ar-plasma treatment is a new strategy for the self-formation of metallic nanostructured arrays over In_2S_3 film surface.

2. Experimental details

2.1. Deposition and plasma treatment conditions of In_2S_3 films

In the present work, In_2S_3 thin films were deposited on glass substrates using vacuum thermal evaporation (HHV BC 300 model) technique at a substrate temperature of 300 °C with the film thickness of 500 nm. Here, In_2S_3 powder (Sigma Aldrich 99.999% purity) was used as source material and evaporated at a rate of 15 Å s^{-1}. Secondly, the as-deposited films were annealed under sulphur ambient at $T_a = 250$ °C for an hour. Further, these annealed films were treated with argon plasma for duration of 30 s using radio frequency inductively coupled plasma (RF ICP) at a radio frequency of 13.56 MHz with RF power of 800 W. At a RF bias power of 100 W, the average ion energy was 75 eV. During UV glow of argon plasma irradiation, the argon gas flow and pressure were maintained at 10 sccm and 0.07 Pa respectively.

2.2. Characterisation techniques

The elemental analysis of In_2S_3 films was studied by energy-dispersive spectroscopy (EDS) with the aid of an INCA Energy attachment (Oxford Instruments). To analyse the surface morphological properties of the films, Hitachi S-4800 and Supra 40 scanning electron microscopes (SEM) were used. The structural properties of In_2S_3 films were studied by using Ultima IV x-ray diffractometer (Rigaku) in grazing incidence x-ray diffraction (GIXD) geometry at 1 degree of incident x-rays with CuK_α radiation source ($\lambda = 1.5418$ Å) scanned in the range of 10° to 80°. The Raman (Raman scattering) spectra were recorded with a Nanofinder High End spectrometer (LOTIS TII) at room temperature. For the excitation source, we used a solid-state laser emitting at a wave length of 532 nm. Optical power was attenuated down to 200 μW to minimise the thermal impact on the samples. Incident beam was focused on the sample surface with a 100× Olympus lens (NA = 0.95), spot diameter was 0.7 μm. Backscattered light was dispersed on a 600 lines mm^{-1} diffraction grating with a spectral resolution better than 3 cm^{-1} and detected using a thermostated CCD matrix with a signal acquisition time equal to 60 s. The transmission and specular reflection (at 8°) spectra of the films were measured using a Photon RT spectrophotometer (Essent Optics) with spectral resolution better than 4 nm using unpolarised light.

3. Results and discussion

3.1. Morphological studies

Figure 1 shows the SEM micrographs of In_2S_3 films. From SEM pictures, it is observed that the film surface was covered with irregular shaped grains for as-deposited films. After annealing, the surface of the films was distributed with large, granular structured grains with well-defined grain boundaries. Moreover, it is observed that the grain size was increased due to the recrystallisation of the films during annealing process in sulphur atmosphere. In case of plasma treated films, an ensemble of nanodroplets are typically formed that are isolated from each other on the surface of the films. During plasma irradiation, as a result of the processes of ion-plasma sputtering of indium sulphide molecules and subsequent deposition of indium atoms on the surface, an ensemble of quasi-spherical or spread droplet shaped nanoparticles are formed (Inset figure 1(c)). The nanodroplets had a size of 20–100 nm in the lateral direction and a height of less than 70 nm. The proofs of the metallic nature of these droplets will be considered in the following sections while analysing the results of EDS and GIXD studies.

3.2. EDS analysis

The elemental composition of In_2S_3 films was studied by EDS and the atomic percentages of 'In' and 'S' in the films are

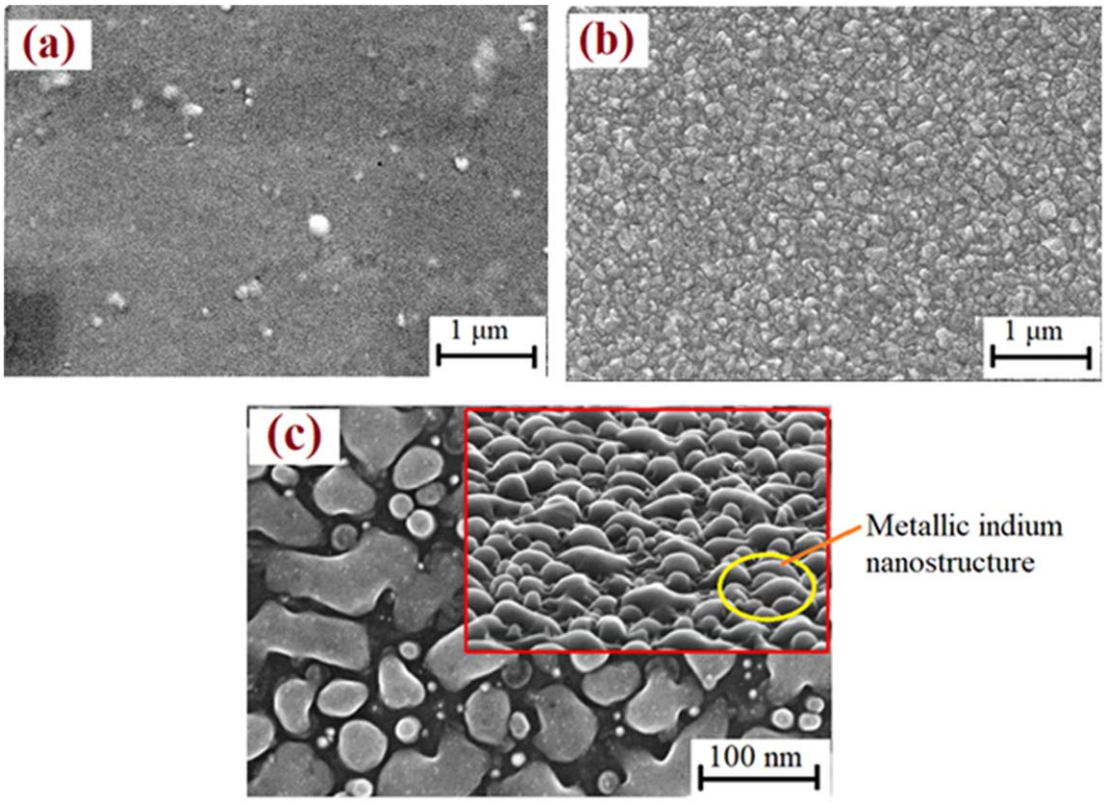

Figure 1. SEM images of In_2S_3 films (a) as-deposited, (b) $T_a = 250\,^{\circ}C$ and (c) plasma treated films [Inset figure taken at a tilt of 70°].

given in table 1. From table 1, it is observed that the as-deposited films are sulphur deficient. This is due to high volatile nature of sulphur, the atoms get re-evaporated from the films at such higher substrate temperatures. In the annealed films, the sulphur content is increased because of rapid reaction of sulphur vapours with indium during annealing process in sulphur atmosphere. Moreover, indium to sulphur (In/S) ratio in the films was observed to be increased from 0.65 to 1.34 after plasma treatment (see figure 2). This result is explained by the fact that the indium sulphide film surface treated with argon ions of energy 100 eV leads to sputtering process of the material at an average rate of $7\,nm\,s^{-1}$. According to [17], the sputtering products of indium sulphide films are In_2S and S_2 molecules, which dissociate into indium and sulphur atoms as a result of exposure to plasma radiation. In this case, the metal atoms are re-deposited on the surface of the film, and the volatile chalcogen atoms leave the sputtering zone. As a result, indium nanodrops are formed on the surface of the In_2S_3 film. Since the EDS method information is taken both from the volume of the film and from the surface, the increase in the In/S ratio after plasma treatment does not contradict the hypothesis of the formation of indium nanodrops on the surface.

Figure 3 shows the schematic representation of formation of indium nanoparticles on In_2S_3 film surface during Ar plasma treatment. When In_2S_3 layer is exposed to Ar plasma, the bombardment of argon ions involves the physical sputtering of surface material [19]. Here, two factors were involved during sputtering process: (i) The film surface temperature reached to 230 °C in 30 s, which is greater than the melting point of indium (150 °C) [20] and (ii) presence of highly intensive UV glow of Ar plasma. Owing to these two factors, the surface of In_2S_3 layer was dissociated into indium and sulphur and due to the highly volatile nature of sulphur, it

Table 1. EDS elemental analysis of In_2S_3 films.

	Atomic content (%)		
	In	S	In/S
Bulk [18]	40.20	59.80	0.67
As-deposited	48.73	51.27	0.95
$T_a = 250\,^{\circ}C$	39.50	60.50	0.65
After plasma treatment	57.44	42.56	1.34

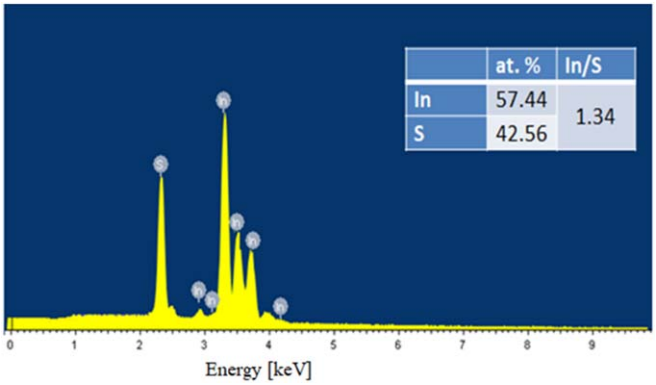

Figure 2. EDS spectrum of In_2S_3 films after plasma treatment.

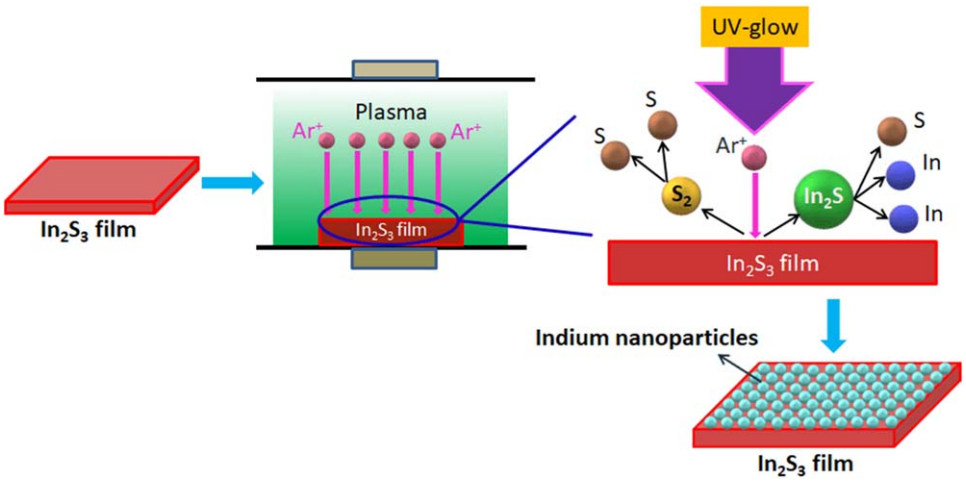

Figure 3. Schematic representation of formation of indium nanoparticles on In_2S_3 film surface upon Ar plasma treatment.

escaped from the reaction zone. Finally, metallic indium settles on the film surface as liquid nanodroplets. Similar dissociation process of In_2S_3 into indium and sulphur was observed by Rodriguez *et al* [17] when the films were treated with nitrogen plasma. The formation of metallic indium nanostructures over In_2S_3 film surface can effectively prevent the photo-corrosion of In_2S_3 by reducing the rapid oxidation of S^{2-} ions during the photocatalytic reaction process in an aqueous solution.

3.3. Structural studies

Figure 4 shows the GIXD patterns of In_2S_3 films. For the as-deposited films, the diffraction peaks observed at $2\theta = 24.96°$, $32.83°$, $38.69°$ and $46.36°$ are corresponding to respective (300), (400), (421) and (521) planes of cubic β-In_2S_3 phase (JCPDS: 32–0456) and (300) plane stands as preferred orientation. Along with these peaks, some minor peaks at $2\theta = 17.02°$ and $18.67°$ corresponding to (112) and (105) planes of tetragonal β-In_2S_3 phase (JCPDS 73–1366) are observed, which is representing the mixed structural phase of the as-deposited films. After annealing the films, the tetragonal phase related planes disappear and the intensity of cubic peaks gets increased due to recrystallisation of the films with (111) plane as preferred orientation. Here in plasma treated In_2S_3 films, the GIXD patterns resemble the same as annealed films but interestingly a small peak of (110) plane related to elemental indium (In) (JCPDS 05–0642) was observed, which supports the presence of metallic indium nanoparticles over In_2S_3 layers as mentioned in the above SEM analysis. In literature, Fu *et al* [21] and other research groups [22–25] observed and reported the benefits of cubic β-In_2S_3 phase rather than tetragonal β-In_2S_3 phase for hydrogen production and stated that the cubic β-In_2S_3 phase has stable photocatalytic activity.

The Raman spectra of In_2S_3 films before and after plasma treatment are presented and compared in figure 5. The Raman spectra of as-deposited films showed certain broad peaks at 98 cm^{-1}, 125 cm^{-1}, 166 cm^{-1}, 266 cm^{-1} which are related to the vibrational modes of β-In_2S_3 phase. In case of annealed

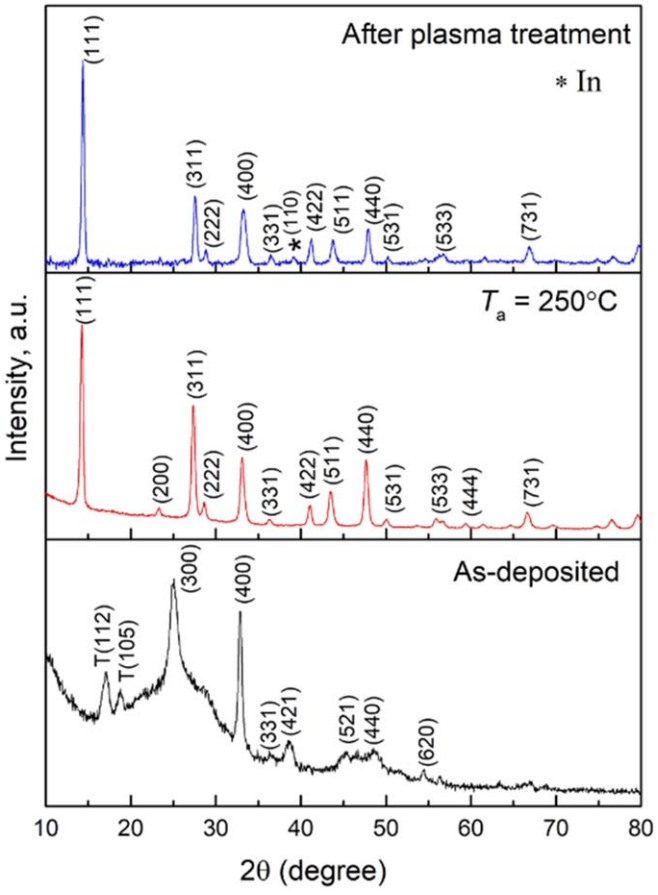

Figure 4. GIXD patterns of In_2S_3 films [*In represents elemental indium].

films, many sharp peaks are observed at 72 cm^{-1}, 92 cm^{-1}, 102 cm^{-1}, 113 cm^{-1}, 135 cm^{-1}, 164 cm^{-1}, 176 cm^{-1}, 245 cm^{-1}, 264 cm^{-1}, 306 cm^{-1}, 326 cm^{-1} and 365 cm^{-1} that are related to β-In_2S_3 phase and are consistent with the previous literature [26–29]. The Raman active modes observed at 245 cm^{-1}, 306 cm^{-1} and 365 cm^{-1} are assigned to A_{1g} mode, while those at 113 cm^{-1}, 176 cm^{-1} and 326 cm^{-1} are assigned to F_{2g} mode and that at 264 cm^{-1} is assigned to E_g

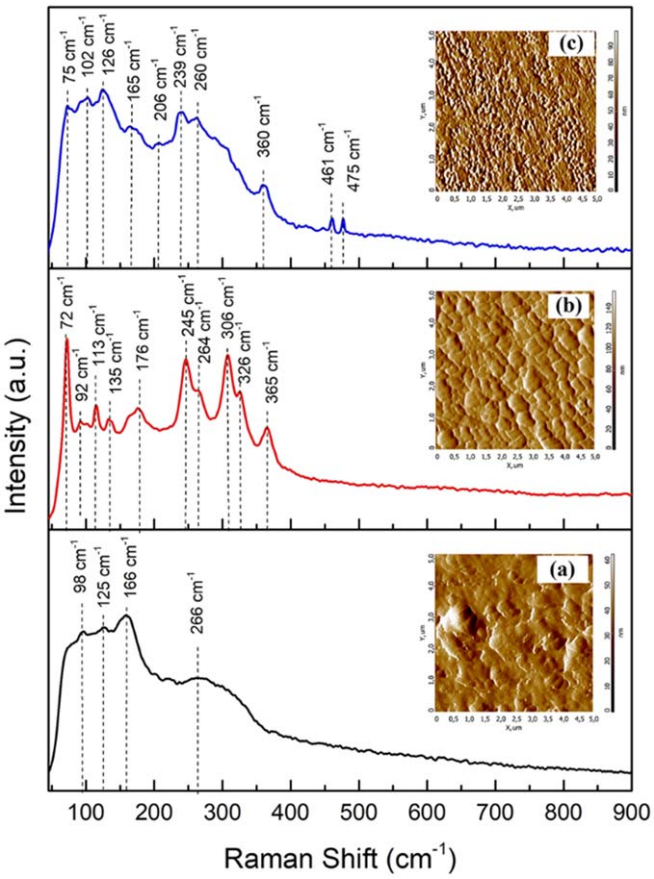

Figure 5. Raman spectrum of In_2S_3 films (a) As-deposited, (b) $T_a = 250$ °C and (c) plasma treated films.

mode of β-In_2S_3 phase [30]. For plasma treated films, weakly expressed peaks of low intensity are observed in the Raman spectrum. Some of the peaks can be attributed to the β-In_2S_3 phase (75 cm^{-1}, 102 cm^{-1}, 126 cm^{-1}, 165 cm^{-1}, 206 cm^{-1}, 239 cm^{-1}, 260 cm^{-1}, 360 cm^{-1} and 365 cm^{-1}), a small (about 5 cm^{-1}) shift of some peaks to the region of lower Raman shifts can be explained by the greater disorder (defectiveness) as a result of plasma exposure. The spectrum also shows peaks in the region of 125 cm^{-1}, 206 cm^{-1}, 289 cm^{-1}, comparable in intensity with the peaks of β-In_2S_3 phase. The lines in the range of 206 cm^{-1} and 289 cm^{-1} are referred to as inactive in Raman but active in IR; their presence in the spectrum can also be explained by disordering of the film structure, as a result of which the forbiddances are not fulfilled [27]. Moreover, two small peaks were observed additionally at 461 cm^{-1} and 475 cm^{-1} in plasma treated films. Here, the peak present at 475 cm^{-1} is related to S-S mode of elemental S [31]. The peak at 461 cm^{-1} can also be attributed to vibrations of sulphur atoms. As stated in [32], the peak at 473 cm^{-1} with a shoulder peak at ~467 cm^{-1} represents S-S bond stretch in the α-S8 ring structure. The article also says that with increasing temperature, the ring structures are destroyed and sulphur polymerises, as evidenced by the peak in the region of 461 cm^{-1}. However, this peak is observed at a temperature of 160 °C, when sulphur is in the liquid phase. In our case, since measurements were carried out at room temperature, the peak at 461 cm^{-1} rather refers to the 'deformed' α-S8 ring, since both lines are slightly offset from the values given in the article.

The inset figures show the AFM images of In_2S_3 films and table 2 below shows the various roughness parameters obtained from the typical AFM data. The surface roughness of the annealed layers was found to be higher than that of the as-deposited layers. The skewness for as-deposited and annealed layers changed from 0.41 to 0.18 and the films had positive skewness, indicating that the films had greater number of peaks than valleys on the surface. Whereas plasma treated films had negative skewness which indicates larger number of valleys than peaks on the surface. Moreover, all the films showed leptokurtic nature (kurtosis value is >3).

3.4. Optical studies

Figure 6 shows the optical transmittance and specular reflectance spectra of In_2S_3 films. Some significant changes were observed in optical transmittance and reflectance of the films upon plasma treatment. The optical transmittance is greatly enhanced to 80% for annealed films compared to as-deposited films. In case of plasma treated films, the optical transmittance is drastically decreased to 15% and reflectance is slightly increased. Since the indium nanostructures are formed over the semiconductor film surface, they partially reflect the incident light in addition to absorption in the bottom semiconductor layer. Therefore, the film is converted from highly transparent film to a light absorber upon plasma irradiation. This type of material can serve as a potential photo-anode for PEC cells for effective production of hydrogen. Gonzalez *et al* [33] also reported such decreasing trend in optical transmittance of CdS thin films upon Ar-plasma treatment.

The optical absorption coefficient (α) was calculated by the following equation [34]:

$$\alpha = -\frac{1}{t}\ln\left(\frac{\sqrt{(1-R)^4 + 4T^2R^2} - (1-R)^2}{2TR^2}\right), \quad (1)$$

where t is the thickness of the films (~0.5 μm), T and R are the transmittance and reflectance, respectively. Figure 7

Table 2. AFM parameters of In_2S_3 films.

Roughness parameters	As-deposited	$T_a = 250$ °C	After plasma treatment
Root mean square (nm)	12	17	10
Roughness average (nm)	8	13	8
Skewness	0.41	0.18	−0.49
Kurtosis	8.9	3.3	3.5

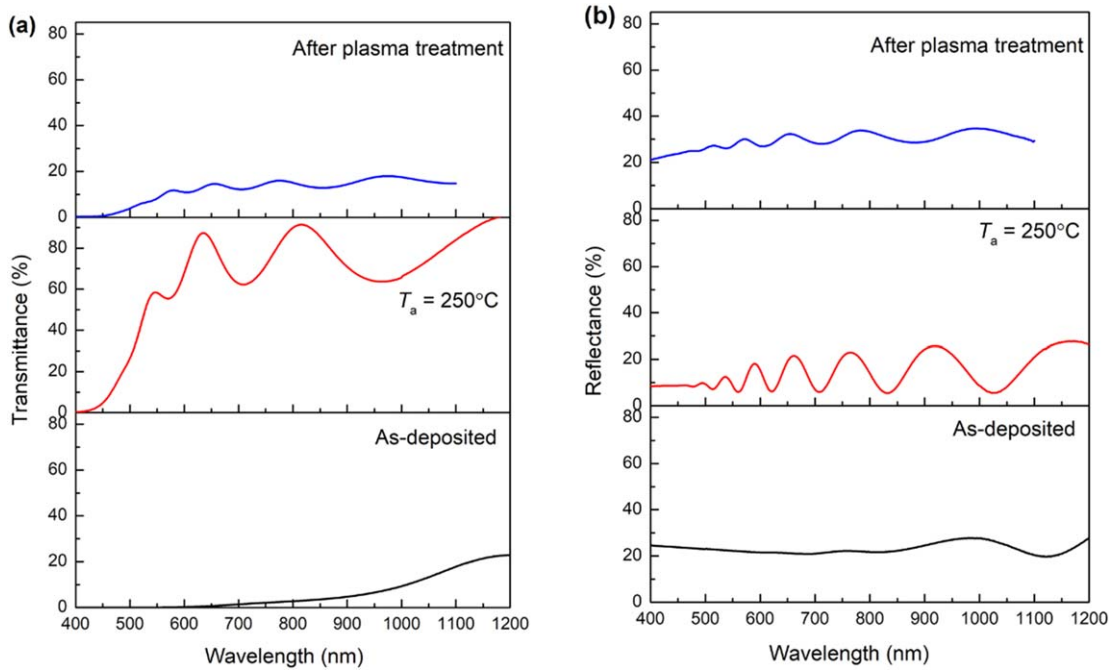

Figure 6. (a) Transmittance and (b) reflectance spectra of In_2S_3 films.

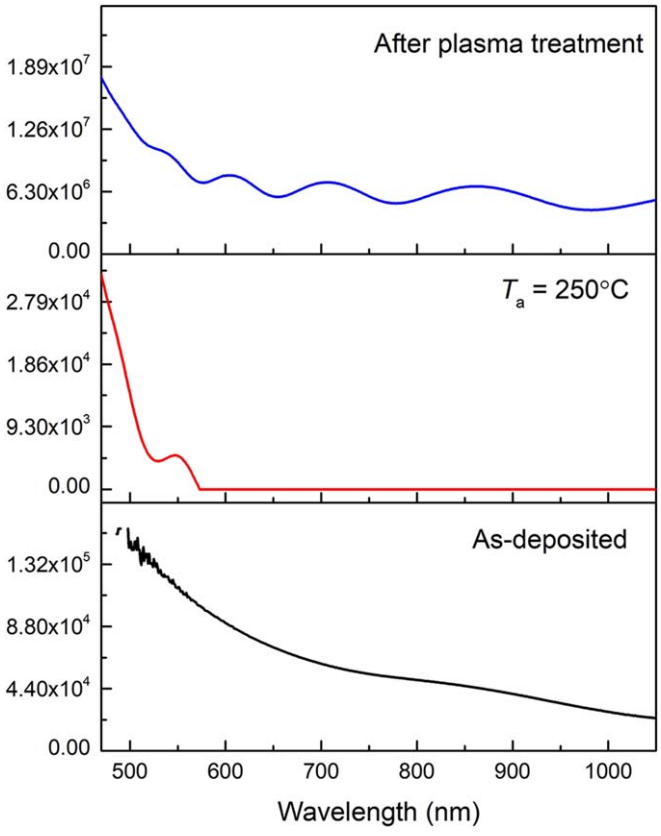

Figure 7. The variation of optical absorption coefficient of In_2S_3 films with incident wavelength.

shows the variation of optical absorption coefficient with incident wavelength for In_2S_3 films. Here, the optical absorption has been enhanced by order of three (from $\sim 10^4$ to $\sim 10^7$ cm^{-1}) for plasma irradiated films due to the presence of indium nanostructure that can enhance the optical path length inside the In_2S_3 layer and effectively trap the incident light. Consequently, the light absorption of the In/In_2S_3 nanostructure hybrid was increased. Wang *et al* [10] observed high optical absorption in the ZnSe nanoribbon/single layer graphene Schottky junction by incorporating the hexagonal plasmonic indium nanoparticles. Cansizoglu *et al* [35] observed that indium sulphide nanorod arrays prepared by glancing angle deposition technique have high optical absorption ($\sim$ 96% for $<$500 nm) compared to conventional thin films ($\sim$79%). Rouf *et al* [36] numerically studied the light trapping mechanism in thin film Si solar cells and observed that the device performance was improved by integrating the indium nanoparticles at front and/or rear surfaces of solar cell compared to the gold nanoparticles.

Figure 8 shows the Tauc plots of In_2S_3 films. The optical energy band gap (E_g) of the films was obtained from $(\alpha h\nu)^2$ versus hν graph by extrapolating the linear portion of the plot onto hν axis. It is observed that the optical energy band gap of In_2S_3 films was enhanced from 1.90 eV to 2.71 eV after annealing. This increment in band gap energy is due to the improvement in the crystallinity with reduced defects [37]. After Ar-plasma irradiation, the value of E_g decreased from 2.71 eV to 2.50 eV. A slight decrease in the band gap width after plasma treatment can be attributed to the well-known fact of an increase in the number of defects in the crystal lattice of a thin film during ion bombardment. Rodriguez *et al* [17] also observed the decrement in E_g values for N_2 plasma treated In_2S_3 films. Similar types of observations were

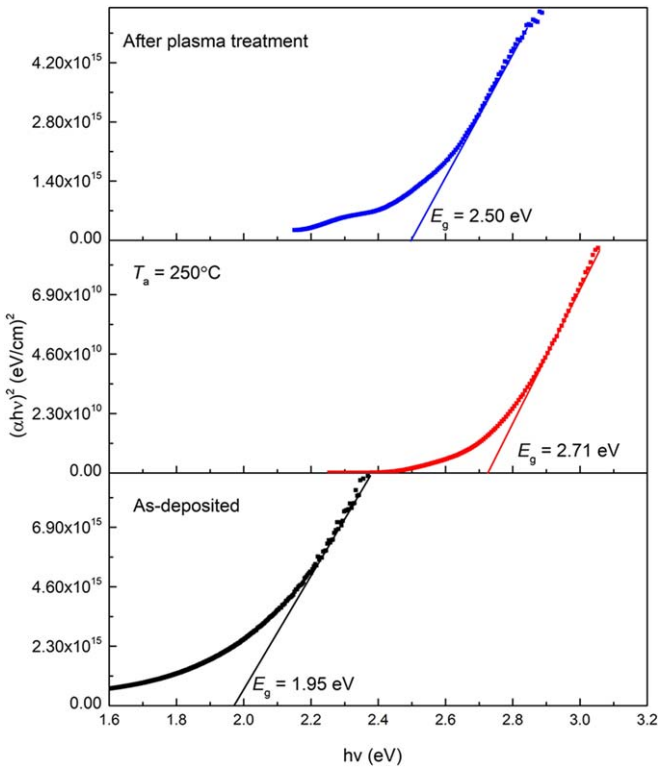

Figure 8. Tauc plots of In_2S_3 films.

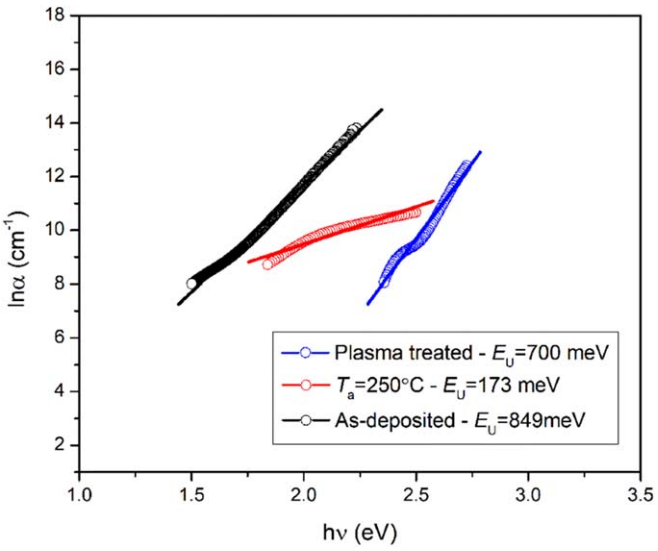

Figure 9. Plot of ln(α) against photon energy ($h\nu$) for In_2S_3 films.

reported for heavy ion irradiated chalcogenide semiconductors by researchers in literature [38–40]. They reported that the decrease in band gap energy of the films is due to the presence of shallow defect levels near the conduction band.

The disorders in the crystal lattice of In_2S_3 films were further analysed by Urbach energy (E_U) calculations following the empirical equation [41]:

$$\alpha = \alpha_0 \exp\left(\frac{h\nu}{E_U}\right), \tag{2}$$

where α_0 is a constant.

Figure 9 shows the linearisation of ln(α) versus hν plot of In_2S_3 films, from which the inverse slope of the plot gives the value of E_U. The lower value of E_U was obtained for annealed films, indicating the presence of less structural disorders and density of localied states in the layers.

4. Conclusion

The present study describes the structural, morphological and optical properties of Ar plasma treated In_2S_3 thin films and the results were compared with as-deposited and annealed films. From SEM micrographs, the surface of annealed films was distributed with large, granular structured grains with well-defined grain boundaries. In case of plasma treated films, an ensemble of indium nanodroplets are typically formed on the surface of the films. From EDS analysis, the indium to sulphur (In/S) ratio in the films was observed to be increased from 0.65 to 1.34 after plasma treatment. The GIXD analysis revealed that the films had cubic β-In_2S_3 phase for both annealed and plasma treated films. From Raman spectra, the Raman modes were related to β-In_2S_3 phase for all the films. Further, the transmittance of In_2S_3 films was greatly reduced and optical absorption was enhanced after plasma treatment. The optical energy band gap of the films was enhanced from 1.90 eV to 2.71 eV after annealing whereas after Ar-plasma treatment, the energy band gap decreased from 2.71 eV to 2.50 eV. The structural disorders in the crystal lattice of In_2S_3 films were further analysed by Urbach energy and the lower value of E_U was obtained for annealed films. In addition, the formation of metallic indium nanostructure over In_2S_3 film surface was the important feature observed after Ar-plasma treatment. The metallic indium nanoparticles loaded on In_2S_3 film surface can form a Schottky barrier, which acts as an electron trap that can effectively prevent the recombination of photo-generated electron-hole pairs. The plasmon induced charge separation in the region of semiconductor/metal interface is more beneficial for the optoelectronic devices. Moreover, the indium nanostructure can serve as catalyst for vapour-liquid-solid growth of different semiconductor nanostructures over indium sulphide films. Hence, Ar-plasma treatment can be an effective way to form a self-nanostructure for chalcogenide materials.

Acknowledgments

The investigation was supported by the Program No: FFNN-2022-0017 of the Ministry of Science and Higher Education of Russia for Valiev Institute of Physics and Technology of RAS and by the Belarusian State Programme for Research 'Physical material science, new materials and technologies'. This work was performed in the framework of R&D initiative of Yaroslavl State University. SEM investigations were carried out at the Facilities Sharing Centre 'Diagnostics of Micro- and Nanostructures' with the support of the Ministry of Science and Higher Education of Russian Federation. The

authors are grateful to A Pipkova and L Mazaletsky for their help in conducting research.

References

[1] Mughal M A, Engelken R and Sharma R 2015 *Sol. Energy* **120** 131
[2] Lee B R and Jang H W 2021 *Electron. Mater. Lett.* **17** 119
[3] Soni V, Raizada P, Kumar A, Hasija V, Singal S, Singh P, Hosseini-Bandegharaei A, Thakur V K and Nguyen V H 2021 *Environ. Chem. Lett.* **19** 1065
[4] Gao W, Liu W, Leng Y, Wang X, Wang X, Hu B, Yu D, Sang Y and Liu H 2015 *Appl. Catal. B : Environ.* **176-177** 83–90
[5] Jayakrishnan R, John T T, Kartha C S, Vijayakumar K, Jain D, Chandra L S and Ganesan V 2008 *J. Appl. Phys.* **103** 053106
[6] Atwater H A and Polman A 2010 *Nature Mater.* **9** 205
[7] Moakhar R S, Gholipour S, Masudy-Panah S, Seza A, Mehdikhani A, Riahi-Noori N, Tafazoli S, Timasi N, Lim Y F and Saliba M 2020 *Adv. Sci.* **7** 1902448
[8] Alkhalayfeh M A, Aziz A A and Pakhuruddin M Z 2021 *Renew. Sustain. Energy Rev.* **141** 110726
[9] Kowalska E 2021 *Catalysts* **11** 410
[10] Verma R, Belgamwar R and Polshettiwar V 2021 *ACS Materials Lett.* **3** 574
[11] Lozano G, Louwers D J, Rodríguez S R K, Murai S, Jansen O T A, Verschuuren M A and Gómez Rivas J 2013 *Light: Sciences & Applications* **2** e66
[12] Fan X, Hao Q, Qiu T and Chu P K 2020 *J. Appl. Phys.* **127** 040901
[13] Wu N 2018 *Nanoscale* **10** 2679
[14] Luo L B, Xie W J, Zou Y F, Yu Y Q, Liang F X, Huang Z J and Zhou K Y 2015 *Opt. Exp.* **23** 12979
[15] Wang Y, Ge C W, Zou Y F, Lu R, Zheng K, Zhang T F, Yu Y Q and Luo L B 2016 *Adv. Optical Matter.* **4** 291
[16] Wang Q, Li J, Bai Y, Lian J, Huang H, Li Z, Lei Z and Shangguan W 2014 *Green Chem.* **16** 2728
[17] Rodriguez M C, Martínez H and Juarez A S 2009 *Thin Solid Films* **517** 2332
[18] El-Nahass M M, Khalifa B A, Soliman H S and Seiam M A 2006 *Thin Solid Films* **515** 1796
[19] Yaxin J, Yufeng O, Zhou Y, Yong Y, Wang D, Chuanpeng Y, Lian L, Zhang Y and Zhao Y 2015 *Surf. Coat. Technol.* **276** 587
[20] Zimin S P, Gorlachev E S, Amirov I I, Naumov V V, Juskenas R, Skapas M, Abramof E and Rappl P H O 2019 *Semicond. Sci. Technol.* **34** 095001
[21] Fu X, Wang X, Chen Z, Zhang Z, Li Z, Leung D Y C, Wu L and Fu X 2010 *Appl. Catalysis* **95** 393
[22] Jrad F, Naceur J B, Ouertani R and Chtourou R 2019 *Physica E* **114** 113585
[23] Chen D and Liu Z 2018 *ACS Sustain. Chem. Eng.* **6** 12328
[24] Han M, Yu L, Chen W, Wang W and Jia J 2016 *Appl. Surf. Sci.* **369** 108
[25] Xu R, Li H, Zhang W, Yang Z, Liu G, Xu Z, Shao H and Qiao G 2016 *Phys. Chem. Chem. Phys.* **18** 2710
[26] Xiong Y, Xia Y, Du G, Tian X and Qian Y 2002 *J. Solid State Chem.* **166** 336
[27] Kambas K, Spyridelis J and Balkanski M 1981 *Phys. Stat. Sol.* (b) **105** 291
[28] Sim Y, Kim J and Seong M J 2016 *J. Alloys Compd.* **685** 518
[29] Horani F and Lifshitz E 2019 *Chem. Mater.* **31** 1784
[30] Alqahtani T, Cernik R J, Brien P O and Lewis D J 2019 *J. Mater. Chem. C* **7** 5112
[31] Izadneshan H and Gremenok V F 2014 *J. Appl. Spectrosc.* **81** (5) 765
[32] Nims C, Cron B, Wetherington M, Macalady J and Cosmidis J 2019 *Sci. Rep.* **9** 7971
[33] Gonzalez G, Krishnan B, Avellaneda D, Alan Castillo G, Das Roy T K and Shaji S 2011 *Thin Solid Films* **519** 7587
[34] Shoroder D K 1990 *Semiconductor materials and device characterization* (New York: Wiley) 3rd edn
[35] Cansizoglu M F, Engelken R, Seo H W and Karabacak T 2010 *ACS Nano* **4** 733
[36] Rouf H K and Dey J 2018 *J. Nano-Electron. Phys.* **10** 06008
[37] Rasool S, Saritha K, Ramakrishna Reddy K T, Tivanov M S, Trofimova A V, Tikoto S E, Bychto L, Patryn A, Malinski M and Gremonok V F 2019 *Curr. Appl Phys.* **19** 108
[38] Kumar P M R, John T T, Kartha C S and Vijayakumar K P 2006 *Nucl. Instr. and Meth.* **244** 171
[39] Choudhary R and Chauhan R P 2017 *Electron. Mater. Lett.* **13** 330
[40] Kamboj M S, Kaur G, Thangaraj R and Avasthi D K 2002 *J. Phys. D: Appl. Phys.* **35** 477
[41] Melsheimer J and Ziegler D 1985 *Thin Solid Films* **129** 35